JCTC Journal of Chemical Theory and Computation

Article

pubs.acs.org/JCTC

Nonadiabatic Dynamics May Be Probed through Electronic Coherence in Time-Resolved Photoelectron Spectroscopy

Kochise Bennett,* Markus Kowalewski,* and Shaul Mukamel*

Chemistry Department, University of California, Irvine, California 92697-2025, United States

ABSTRACT: We present a hierarchy of Fermi golden rules (FGRs) that incorporate strongly coupled electronic/nuclear dynamics in time-resolved photoelectron spectroscopy (TRPES) signals at different levels of theory. Expansion in the joint electronic and nuclear eigenbasis yields the numerically most challenging exact FGR (eFGR). The quasistatic Fermi Golden Rule (qsFGR) neglects nuclear motion during the photoionization process but takes into account electronic coherences as well as populations initially present in the pumped matter as well as those generated internally by coupling between electronic surfaces. The standard semiclassical Fermi Golden Rule (scFGR) neglects the electronic coherences and the nuclear kinetic energy during the ionizing pulse altogether, yielding the classical Condon approximation. The coherence contributions depend on the phase-profile of the ionizing field, allowing coherent control of TRPES signals. The photoelectron spectrum from model systems is simulated using these three levels of theory. The eFGR and the qsFGR show temporal oscillations originating from the electronic or vibrational coherences generated as the nuclear wave packet traverses a conical intersection. These oscillations, which are missed by the scFGR, directly reveal the time-evolving splitting between electronic states of the neutral molecule in the curve-crossing regime.

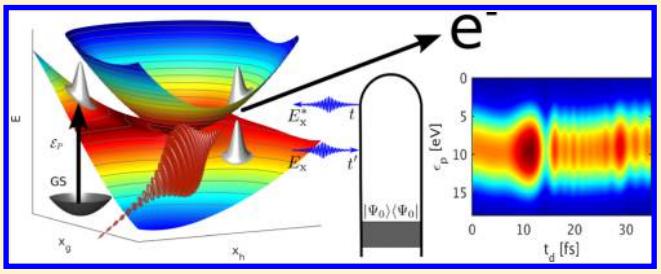

1. INTRODUCTION

Photoelectron spectroscopy[1] (PES), in which the kinetic energy of electrons liberated from a sample via interaction with light is measured, has long been utilized to gain knowledge of the level-structure of molecules and materials. Energy conservation implies that the photoelectron energy is indicative of the difference between the frequency of ionizing radiation and the ionization potential of the material. More recently, the technique has been extended to the time-domain. In time-resolved photoelectron spectroscopy[2] (TRPES), a pump pulse prepares the molecule in a nonstationary state, the dynamics of which are subsequently tracked by varying the delay time between the pumping pulse and a subsequent ionizing XUV or X-ray pulse, the detected quantity being the energy-resolved (or energy integrated) photoelectron yield. With the advent of ultrashort pulses, such experiments are able to achieve femtosecond resolution of excited state dynamics, allowing one to stroboscopically track ultrafast photochemical processes and nuclear dynamics.

Special attention has been drawn to the nonadiabatic dynamics through Conical Intersections (CoIns) due to their broad impact on photochemical and even photobiological processes.[3−7] CoIns provide ultrafast, nonradiative decay pathways which influence product yields and reaction rates in virtually all photochemical processes. Near a CoIn, the nuclear and electronic degrees of freedom become strongly coupled, and the Born−Oppenheimer approximation (BOA), which is based on the separation of electronic and nuclear frequencies, breaks down.[8,9] The passage through a CoIn can be detected by vibrational spectroscopic signatures,[10−13] fast population dynamics,[3,14] and TRPES.[15,16] However, with shorter pulses in the attosecond regime available, measuring[17] and even controlling the electronic dynamics[18] becomes possible. With the increasing availability of ultrashort pulses from high harmonic generation sources[19,20] and free electron lasers,[21] novel techniques based on a direct measurement of the electronic coherence become feasible.[22,23]

The nuclear coupling in the CoIn-region transfers population between the electronic states, while also generating coherences between them. In this paper, we show that TRPES with subfemtosecond pulses can be utilized to detect the electronic coherence created by the non-BOA coupling encountered by a nuclear wavepacket as it passes through the region of a CoIn. Multimode wave packet simulations of the TRPES of pyrazine[24,25] show that the time-dependence is essentially an overlay of electronic population with coherent nuclear dynamics, the latter of which produces oscillations at nuclear frequencies. This result can be well-understood from the perspective of a semiclassical Fermi Golden Rule (scFGR, eq 5) in which the contributions from the various adiabatic electronic surfaces add incoherently, weighted by their time-dependent populations. The scFGR is intuitive and frequently employed to simulate and interpret spectra.[15,16,26] It is applicable in the BOA, where the electronic states do not couple. However, the non-BOA coupling that redistributes electronic population also generates electronic coherence, even if none is initially produced by the pumping process. We show that these

Received: August 26, 2015
Published: December 21, 2015

DOI: 10.1021/acs.jctc.5b00824
J. Chem. Theory Comput. 2016, 12, 740−752

electronic coherences result in oscillations in the signal intensity that are missed in the standard scFGR expressions. Under certain conditions, the period of these oscillations is indicative of the average energy separation between the neutral electronic potential surfaces. This effect has been reported from experiments in the NO molecule,[27] which showed subpicosecond oscillations. New subfemtosecond light XUV and X-ray light sources can access the appropriate time-domain to observe this effect in polyatomic molecules with larger energy separations.

This paper focuses on demonstrating the signatures of electronic coherence in the TRPES signals generated by subfemtosecond pulses. We provide a novel formalism, which allows for inclusion of the electronic coherences and show how well effects are reproduced by the various simulation protocols with model systems. The paper is organized as follows. In section 2, we describe the model and the semiclassical Fermi golden rule for TRPES. In section 3, we obtain an exact correlation-function expression for the signal as well as a corresponding exact FGR, written as an expansion in the eigenbasis. From these exact expressions, we then rigorously derive the scFGR in section 4 by making the quasi-static approximation. In the process we obtain, an additional class of terms, arising from the electronic coherences. We discuss under what conditions these terms must be accounted for and what information they carry. In sections 5 and 6, we compare the features of the different levels of approximation using simulations for model systems.

2. FERMI'S GOLDEN RULE FOR TRPES

We describe TRPES with a Hamiltonian of the form discussed in ref 28, which neglects the interaction between the ionized molecule and the photoelectron. We work in the adiabatic basis and consider a set of neutral electronic states (labeled by a, b) and ionized electronic states (labeled by α). The nuclear kinetic energy operator ($\hat{T}$) generates nonadiabatic coupling between the neutral electronic states. This coupling is responsible for population transfer between electronic states and also generates coherences that can impact the signal, as we will show. For simplicity, we only consider such coupling in the neutral molecule. We therefore write the total Hamiltonian as

$$\hat{H} = \hat{H}_{\mathrm{M}} + \hat{H}_{\mathbf{p}} + \hat{H}_{\mathrm{x}}(t) \tag{1}$$

We assume that the pumping process bringing the system to a nonstationary state is temporally well-separated from the probing X-ray pulse. Thus, we have omitted the interaction with the pumping field for simplicity. The molecular Hamiltonian is

$$\hat{H}_{\mathrm{M}} = \sum_{a} |a\rangle(\hat{T}_a + \hat{E}_a)\langle a| + \sum_{a,b} |a\rangle\hat{T}_{ab}\langle b| + \sum_{\alpha} |\alpha\rangle(\hat{T}_\alpha + \hat{E}_\alpha)\langle\alpha| \tag{2}$$

with $\hat{E}_a$ ($\hat{E}_\alpha$) is the energy of the a-th (α-th) adiabatic electronic state of the neutral (ionized) molecule, and $\hat{T}$ is the nuclear kinetic energy operator which couples states in the neutral species. Nonadiabatic couplings between ionized states are ignored. All of these quantities are therefore operators in the nuclear subspace (as indicated by the circumflexes). Following ref 28, we utilize a second-quantized description of the photoelectron states and a first-quantized description of the bound states. This facilitates our treatment of PES in analogy with spontaneous light emission and the inclusion of molecule-photoelectron interactions (the latter are beyond the scope of this paper and not included in our model). We take the photoelectron states to be independent of the nuclei and assume they do not interact with the ion (justified for sufficiently high-energy photoelectrons) and therefore write

$$\hat{H}_{\mathbf{p}} = \sum_{\mathbf{p}} \varepsilon_{\mathbf{p}} \hat{c}_{\mathbf{p}}^{\dagger} \hat{c}_{\mathbf{p}} \tag{3}$$

for the photoelectron Hamiltonian ($\hat{c}_{\mathbf{p}}^{\dagger}$, $\hat{c}_{\mathbf{p}}$ are Fermi creation/annihilation operators for free photoelectrons with energy $\varepsilon_{\mathbf{p}}$). Note that the formalism can be straight-forwardly applied to photo detachment[29] as well, which only differs in the initial and final states (anion to neutral).

We work in the direct product space of bound (molecular) and continuum (photoelectron) states, and the interaction with the photoionizing X-ray pulse is then written as

$$\hat{H}_{\mathrm{x}}(t) = -E_{\mathrm{x}}(t) \sum_{\mathbf{p}\alpha a} \hat{\mu}_{\mathbf{p}\alpha,a} \hat{c}_{\mathbf{p}}^{\dagger} |\alpha\rangle\langle a| + \hat{\mu}_{\mathbf{p}\alpha,a}^{\dagger} \hat{c}_{\mathbf{p}}^{\dagger} |a\rangle\langle\alpha| \tag{4}$$

where $E_x(t)$ is the ionizing X-ray pulse envelope. Throughout, we work in the interaction picture with respect to $\hat{H}_{\mathrm{int}}(t) = \hat{H}_x(t)$ and use atomic units, setting $\hbar = m_e = e = 1$. The electronic matrix elements of the transition dipole remain operators in the nuclear space, as indicated. For simplicity, we assume that $\hat{\mu}$ is independent of the momentum $\mathbf{p}$, which is a reasonable approximation for fast photoelectrons,[30] but not for slow electrons which do interact with the ion.

The photoelectron spectrum obtained via ionization by an X-ray pulse with frequency ω_x and arrival time t_d is most commonly simulated using the scFGR[16]

$$\begin{aligned} S_{\mathrm{sc}}(\varepsilon_{\mathbf{p}}, t_d) &= \int d\omega_{\mathrm{x}} |E_{\mathrm{x}}(\omega_{\mathrm{x}})|^2 S_{\mathrm{scFGR},0}(\varepsilon_{\mathbf{p}}, t_d, \omega_{\mathrm{x}}) \\ S_{\mathrm{sc},0}(\varepsilon_{\mathbf{p}}, t_d, \omega_{\mathrm{x}}) &= \sum_{a\alpha} \langle |\mu_{\alpha a}(\{\mathbf{q}\}(t_d))|^2 \rho_{aa}(\{\mathbf{q}\}(t_d)) \\ &\quad \times \delta(\varepsilon_{\mathbf{p}} - \omega_{\mathrm{x}} + \mathcal{E}_\alpha(\{\mathbf{q}\}(t_d)) - \mathcal{E}_a(\{\mathbf{q}\}(t_d)))\rangle \end{aligned} \tag{5}$$

where $\{\mathbf{q}\}(t)$ is the time-dependent set of nuclear coordinates (now written explicitly since they are computed classically), and $\langle ... \rangle$ indicates an averaging over these coordinates. This averaging can be done at various levels of theory (ab initio multiple spawning,[31] surface hopping,[32] etc.). Below, we will derive a fully quantum-mechanical version of the scFGR, in which the averaging comes as expectation values taken over the time-dependent nuclear wave function. This derivation will clarify the origin and applicability regime of eq 5 while naturally generating additional terms proportional to the electronic coherence ρ_{ab}. Note that eq 5 only contains terms proportional to the populations ρ_{aa} and the signal is solely dependent on the power spectrum of the ionizing X-ray pulse $|E_x(\omega)|^2$. In contrast, the coherence terms appear with $E_x(\omega)E_x^*(\omega')$, which can be manipulated by on the phase of the ionizing field.

3. THE EXACT TIME DEPENDENT PHOTOELECTRON SIGNAL

We follow the microscopic treatment outlined in refs 28 and 33 and define the photoelectron signal as the energy-resolved, integrated rate of change of the number of photoelectrons which gives the total energy-resolved photoelectron yield. This results in (see Appendixes A and B)

DOI: 10.1021/acs.jctc.5b00824
J. Chem. Theory Comput. 2016, 12, 740−752

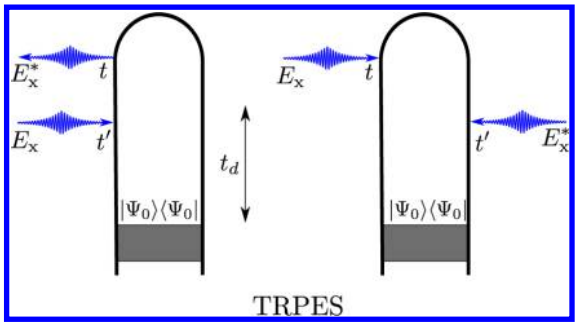

Figure 1. Two loop diagrams for the TRPES signal (eq 22). Since the usual rules for loop diagrams maintain time-ordering, we show these two loops rather than a single loop with unrestricted times as would be implied by eq 6.

$$S_e(\varepsilon_p, t_d) = \int dt \int dt' \tilde{E}_x^*(t)\tilde{E}_x(t')e^{-i(\varepsilon_p-\omega_x)(t-t')}\langle\hat{\mu}(t)\hat{\mu}^\dagger(t')\rangle_0 \tag{6}$$

where $\langle\ldots\rangle_0$ indicates an expectation value with respect to the initial state $|\Psi(t_0)\rangle = |\psi(t_0)\rangle\otimes|\phi(t_0)\rangle$ with ψ_0 and ϕ_0 the initial electronic and nuclear wave functions. The assumption of a product state form for the initial total wave function is justified when a single excited electronic state can be targeted by the pumping process, but the generalization to a sum of such product states is straightforward if less succinct. The "e" subscript stands for "exact" and serves to differentiate it from the various approximate expressions defined below. In the above equation, the photoelectron part of the dipole correlation has been evaluated (this is possible since $[\hat{H}_p, \hat{H}_M] = 0$) and $\hat{\mu}(\hat{\mu}^\dagger)$ "annihilates" ("creates") the ion

$$\hat{\mu} \equiv \sum_{\alpha a} \hat{\mu}_{\alpha a}^\dagger |a\rangle\langle\alpha| \tag{7}$$

We note that eq 6 assumes a uniform density of photoelectron states and will only be physical for $\varepsilon_p > 0$. This can be ensured by shifting the carrier frequency of the ionizing pulse. We have also expanded the electric field amplitiudes into their positive and negative frequency components with carrier frequencies $(\tilde{E}_x^{(*)}(t)e^{\mp i\omega_x t})$ and kept only the rotating-wave terms. Equation 6 is the most straighforward way to simulate the time-resolved photoelectron spectrum, and this will be done for a model system in sections 5 and 6.

The molecular dipole correlation function in eq 6 can be straightforwardly expanded in the eigenstates of $\hat{H}_M$ in the full nuclear+electronic space. Indexing such states by i, j, k, ... and expanding the initial wave function $|\Psi_0\rangle = \sum_i c_{i0}|i\rangle$, we obtain

$$\begin{aligned} S_e(\varepsilon_p, t_d) &= \sum_k |\sum_i c_{i0}\mu_{ki}\tilde{E}_x(\varepsilon_p - \omega_x - \varepsilon_i + \varepsilon_k)|^2 \\ &\to \sum_{ki} \rho_{ii}|\tilde{E}_x\mu_{ki}|^2\delta(\varepsilon_p - \omega_x - \varepsilon_i + \varepsilon_k) \end{aligned} \tag{8}$$

where the last relation follows on assumption of a mixed state with population of state i given by ρ_{ii} (electronic decoherence to such a mixed state can be described more rigorously in Liouville space[28]) and assuming a narrow-band pulse power spectrum. This exact Fermi Golden Rule (eFGR) in the full nuclear+electronic space is always possible to write but difficult to implement. The difficulty lies in the calculation of the eigenstates which is numerically intractible for all but the simplest systems. This form does however reveal that TRPES can be written as a sum of squares of transition amplitudes and is thus positive-definite (as must physically be the case). Also of note is the fact that the signal consists of an incoherent sum of exact population terms that do not mix; population transfer does not occur. Of course, this is a special property of the eigenbasis and does not generally hold for the product-state (adiabatic or diabatic) bases. This is of particular importance for CoIns since the "good basis" becomes "bad" near the CoIn as the BOA breaks down and the nuclei couple different electronic states.

It is important to note that expressions formally equivalent to eq 23 can also be obtained by calculating the expectation value of the photoelectron population for any time after the passage of the ionizing pulse. This is easily seen from the fundamental theorem of calculus on eq 19 and the initial condition of no photoelectrons.[24,25] We have presented this slightly different derivation to highlight the relationship with transient absorption and other heterodyne-detected signals, which are derivable from the integrated rate-of-change of the photon number.

For comparison to the eFGR, it will be useful to also develop an understanding for the separate roles that electronic populations and coherences play in eq 6 (note that populations and coherences are basis-dependent and we refer here to the adiabatic basis as opposed to the full eigenbasis which is not practial to utilize). To that end, we rewrite eq 6 using eq 7 as

$$\begin{aligned} S_e(\varepsilon_p, t_d) = \int dt \int dt' \tilde{E}_x^*(t)\tilde{E}_x(t')e^{-i(\varepsilon_p-\omega_x)(t-t')} \\ \times \Big(\sum_{a\alpha} \langle\hat{M}_{a0}^*(t)\hat{\mu}_{\alpha a}\hat{M}_{\alpha\alpha}(t-t')\hat{\mu}_{\alpha a}^\dagger\hat{M}_{a0}(t')\rangle_{\phi_0} \\ + \sum_{a\neq b,\alpha} \langle\hat{M}_{b0}^*(t)\hat{\mu}_{\alpha b}\hat{M}_{\alpha\alpha}(t-t')\hat{\mu}_{\alpha a}^\dagger\hat{M}_{a0}(t')\rangle_{\phi_0}\Big) \end{aligned} \tag{9}$$

In the above, we have defined the electronic transition amplitudes

$$\begin{aligned} \hat{M}_{a0}(t) &= \langle a|e^{-i\hat{H}_M t}|\psi_0\rangle \\ \hat{M}_{\alpha\alpha}(t) &= \langle\alpha|e^{-i\hat{H}_M t}|\alpha\rangle \end{aligned} \tag{10}$$

where the expectation values are now solely over the initial nuclear wave function. The assumption of no coupling between ionized electronic states of the molecule prevents us from having to consider such terms as $\hat{M}_{\beta\alpha}(t)$ for $\beta \neq \alpha$.

The first term in eq 9 represents the contribution of electronic populations, while the second term contains the coherence contributions. If the state initially prepared by the pump contains no electronic coherences and the states $|a\rangle$ do not mix during the time propagation (they are eigenstates in the electronic subspace and the BOA holds), then the coherence terms would vanish by orthogonality. If either of these conditions is violated, the coherences must be accounted for.

4. THE QUASISTATIC APPROXIMATION

To obtain the final FGR-like expression, we will substitute the temporal field envelopes in eq 9 for their Fourier transforms and approximate the nuclei as static during interaction with the ionizing pulse. This gives the quasi-static Fermi Golden Rule (qsFGR)

$$S_{qs}(\varepsilon_p, t_d) = S_{qs}^{pop}(\varepsilon_p, t_d) + S_{qs}^{coh}(\varepsilon_p, t_d) \tag{11}$$

DOI: 10.1021/acs.jctc.5b00824
J. Chem. Theory Comput. 2016, 12, 740−752

$$S_{\mathrm{qs}}^{\mathrm{pop}}(\varepsilon_{\mathbf{p}}, t_d) = \sum_{a\alpha} \rho_{aa}(t_d)|\mu_{\alpha a}(t_d)\tilde{E}_{\mathrm{x}}(\varepsilon_{\mathbf{p}} - \omega_{\mathrm{x}} + \mathcal{E}_{\alpha}(t_d) - \mathcal{E}_{a}(t_d))|^2 \tag{12}$$

$$\begin{aligned} S_{\mathrm{qs}}^{\mathrm{coh}}(\varepsilon_{\mathbf{p}}, t_d) = \sum_{a\neq b,\alpha} & \rho_{ab}(t_d)\langle\phi_{\alpha b}(t_d)|\phi_{\alpha a}(t_d)\rangle\mu_{\alpha b}(t_d)\mu_{\alpha a}^{\dagger}(t_d) \\ & \times \tilde{E}_{\mathrm{x}}^{*}(\varepsilon_{\mathbf{p}} - \omega_{\mathrm{x}} + \mathcal{E}_{\alpha}(t_d) - \mathcal{E}_{b}(t_d)) \\ & \times \tilde{E}_{\mathrm{x}}(\varepsilon_{\mathbf{p}} - \omega_{\mathrm{x}} + \mathcal{E}_{\alpha}(t_d) - \mathcal{E}_{a}(t_d)) \end{aligned} \tag{13}$$

where we have replaced $c_a(t)c_b^*(t) = \rho_{ab}(t)$ for the electronic populations ($a = b$) and coherences ($a \neq b$) and explicitly separated the population and coherence terms ($\mathcal{E}_b$ and μ_{ab} are defined in analogy with eqs 39 and 40). This is a FGR type expression in the electronic space where the time dependence due to expectation values is taken over the time-dependent nuclear wave packet as opposed to the full nuclear+electronic space. Since the summations in eq 11 contain far fewer terms than those in eq 8, this expression is much more tractable. On the other hand, it includes terms that are absent from the scFGR (eq 5). The scFGR is an approximation to the population part of the qsFGR (eq 12), which we term the quasi-static population Fermi Golden Rule (qspFGR) in which the nuclear propagation is treated semiclassically to obtain the time-dependence of the parameters (energies, dipoles, and populations).

Arriving at eq 9 entails no loss of generality. The key approximation, which is reflected in eqs 35−36 and 38−40, is that the molecule interacts with the ionizing X-ray pulse faster than the nuclei can appreciably move (the quasistatic approximation) and that the time scale of nuclear motion is much longer than the coherent electronic oscillation period. This breaks down in the vicinity of a CoIn where the electronic energy gap vanishes. We have thus arrived at four versions of the FGR: (1) The exact FGR in the nuclear+electronic space (eq 8), which does not mix populations (specifically, $|\psi_0\rangle = |i\rangle \Rightarrow |\psi(t)\rangle \propto |i\rangle$) since it is written in the eigenbasis. (2) The "quasistatic" FGR, which approximates the correlation function (from which the eFGR was obtained) by assuming frozen nuclei during the ionizing pulse in order to obtain an intuitive formula similar to the eFGR but in a more numerically tractable basis. (3) The "quasistatic population" FGR (qspFGR), which neglects the electronic coherences in the qsFGR. (4) The "semiclassical" FGR (eq 5) which approximates the qspFGR. Equation 12 still contains expectation values of the electronic energies taken over the exact nuclear wave function. Although this is an improvement over eq 8 (since the nuclear wave function can be numerically propagated without obtaining the exact eigenstates), eq 12 is still commonly approximated as in eq 5 by taking the nuclei as classical objects moving stochastically and then averaging over the resulting trajectories.

In this hierarchy of golden rules, the latter two (eqs 12 and 5) appear nearly identical, and very similar to the exact (eq 8). However, as we remarked earlier, the latter two are written in a product adiabatic basis rather than the exact nuclear+electronic eigenbasis. While this make simulations easier due to the smaller number of terms in the summation, it also means that the states can couple and will generally mix. This mixing will transfer electronic population between states while generating electronic coherences (eq 13). While the quasi-static assumption of frozen nuclei during the ionization process may be well-justified for ultrashort pulses, dropping the electronic coherence terms is not justified when coherences are internally generated by the propagation due to the breakdown of the BOA and the coupling of electronic states through the nuclei. We have thus shown that the FGR approach can easily be extended by the inclusion of coherence terms (eq 13) to obtain the more general qsFGR (eq 11). This allows the effects of electronic coherence on the TRPES signal to be calculated at a similar computational cost to the commonly employed scFGR. In section 5, we will explore the consequences of these internally generated coherences and what information may be obtained from their contribution to the signal.

We now examine more closely eq 13, which encodes the coherence contributions to TRPES within the quasistatic approximation. It is apparent that, while the population terms depended on the power spectrum $|\tilde{E}_{\mathrm{x}}(\omega)|^2$, the coherence terms depend on the frequency-dependent phase of the ionizing pulse via $\tilde{E}_{\mathrm{x}}^{*}(\omega)\tilde{E}_{\mathrm{x}}(\omega')$, opening up another avenue of control for these signals. Also of note is the nuclear coherence factor $\langle\phi_{\alpha b}(t_d)|\phi_{\alpha a}(t_d)\rangle$ (missing from the populations since the nuclear wave packets are normalized). This factor represents the overlap of the nuclear wave packet on state a at time t_d with that on state b. Since the two potential surfaces are typically different, the two wave packets will generally not overlap appreciably after some time. This factor therefore adds a decay that complicates the observation of the coherence terms and can justify their exclusion, as in the scFGR, when the decay is sufficiently fast relative the delay times t_d. This is ordinarily the case, for example, in slow picosecond TRPES but is not generally true in the ultrafast regime. In a more comprehensive treatment, nuclear movement during ionization, as well as spectator modes, would further decohere these terms. While these effects are important, they are not the primary interests of this paper.

As will be illustrated in the next section, the most visible signature of the coherence terms in TRPES is a characteristic oscillatory pattern in the t_d-dependence of the electronic coherence $\rho_{ab}(t_d)$. The frequency of this beating pattern allows one to determine the separation between states a, b without direct spectral resolution. In principle, the actual oscillation period is related to the eigenenergies, which complicates the interpretation of the beating pattern in the region of the CoIn. Once the nuclear wave packet is sufficiently far from the CoIn for the intersurface coupling to be small relative to the electronic energy separation, the frequency can safely be interpreted as corresponding to the gap. In our models, we find that the onset of this regime is relatively rapid (within a few fs of the wave packets arrival at the CoIn). In this sense, the CoIn acts as a scatterer that transfers population between the two electronic states but also sets in motion a coherent oscillation.

Finally, we note that, if one simply invokes the reasonable approximation that $\rho_{ab}(t_d) \sim \rho_{ab}e^{-i\omega_{ab}t_d}$, we can transform $a \leftrightarrow b$ and combine terms to get

$$S_{\mathrm{qs}}^{\mathrm{coh}}(\varepsilon_{\mathbf{p}}, t_d) \sim \sum_{ab} \cos(\omega_{ab}t_d) \tag{14}$$

where we have dropped all other factors inside the summation. This term is clearly not positive-definite, and the coherence term can therefore both enhance or suppress the population term in the photoelectron signal. Thus, the presence of coherence can suppress or enhance the "primary" photoionization process from populations. This can be understood as the presence of the coherence opening up new pathways that

DOI: 10.1021/acs.jctc.5b00824
J. Chem. Theory Comput. 2016, 12, 740−752

interfere destructively or constructively with the population ionization pathways.

5. COMPARISON OF THE FGR EXPRESSIONS

In this section, we will simulate the TRPES signal for a model involving a single nuclear coordinate with the various FGR expressions as well as with eq 6. The correlation function expression implicitly includes both population and coherence contributions, as can be seen from its expanded form in eq 9, and, combined with a state propagation scheme, offers an exact way to simulate the full TRPES signal. Rather than specifying the adiabatic potential surfaces, we will work from the outset in the diabatic basis. This simplification to a scalar coupling retains the essential physics of an intersurface coupling in the region of a degeneracy and the population transfer and coherence creation that follows from such coupling. We assume three relevant electronic states, two un-ionized (labeled $|1\rangle$ and $|2\rangle$) and one ionized ($|3\rangle$). The two un-ionized states intersect and are coupled near the intersection point, and all three surfaces are taken to be harmonic with the same shape. This is the simplest model that can illustrate the effect of electronic coherences on TRPES signals and will serve as a readily comprehensible test case. The Hamiltonian in the diabatic basis reads

$$\hat{H}_{\mathrm{M}} = \sum_{j=1}^{3} |j\rangle(\hat{T}_j + \hat{V}_j)\langle j| + |1\rangle\hat{V}_{12}\langle 2| + |2\rangle\hat{V}_{21}\langle 1| \tag{15}$$

where $\hat{T}_j \equiv -\frac{1}{2m}\frac{d^2}{dx^2}$, the nuclear kinetic energy operator, is now diagonal in the electronic space (see Appendix A for parameters). We give all three diabatic surfaces the same curvature to maximize the coherence time which is limited by the nuclear wave function overlap.

The initial wavepacket (assumed to be on surface 1 initially) as well as all potential surfaces and the intersurface coupling are displayed in Figure 2(top). We then propagate this initial wavepacket using a Short Iterative Lanczos (SIL) scheme[34] and calculate the two-time dipole correlation function, working in the Condon approximation and taking all dipole elements to be unity for simplicity. More rigorous treatment of μ can be approximated for example by Dyson orbitals,[35] which introduce weight factors for different ion states as well as angular distributions. The time-dependent populations of the neutral electronic states and the magnitude of their coherence are plotted in Figure 2(Bottom). Taking the ionizing pulse to be a Gaussian with central time t_d, standard deviation σ_T, and carrier frequency $\omega_x(E_x(t) = e^{-((t-t_d)^2/(2\sigma_t^2))}e^{-i\omega_x t})$, we calculate eq 6 and compare to the qspFGR result (eq 12) in Figure 3. This comparison immediately reveals the presence of coherent oscillations in the directly propagated signal that are absent in the approximate FGR result. This failure of the qspFGR is due to the fact that the electronic states (whether adiabatic or diabatic) are not eigenstates of the molecular Hamiltonian. The coupling $\hat{V}_{12}$ couples un-ionized electronic states, and the propagator therefore mixes them. This renders the coherence term in eq 9 finite, and we must go beyond the qspFGR/scFGR.

Although the restricted time window used to capture the ultrafast dynamics has left us with insufficient spectral resolution to directly resolve the two un-ionized surfaces, the beating pattern reveals their splitting. A visual inspection of the coherent oscillations reveals a period of roughly 10 fs. The

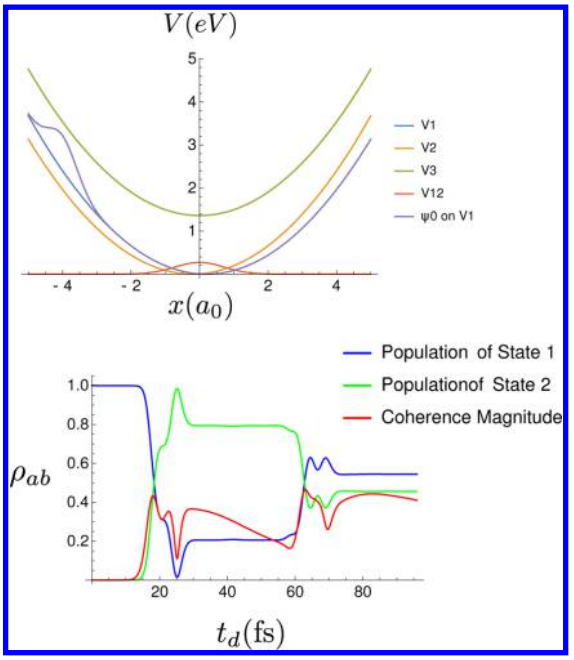

Figure 2. (Top) Nuclear dependence of the diabatic electronic energies including the potential coupling the two un-ionized surfaces. The initial nuclear wavepacket (rescaled for visualization) on the V_1 surface. (Bottom) The populations and coherence magnitude for the un-ionized adiabatic states for the first 96 fs. It is noteworthy that the coherence remains appreciable relative to the populations for some time after its creation.

average separation between un-ionized electronic surfaces from t_d = 45 fs to t_d = 65 fs (roughly the time from first peak to last peak in the oscillation pattern) corresponds to a beating period of 9.74 fs, a relative error of only 2.6%.

In deriving eq 12, we have made the quasistatic approximation, where we neglected the kinetic energy for the duration of the ionizing pulse as well as the contribution from electronic coherences. To investigate the relative importance of these two approximations, we also have computed separately the first term in eq 9, which neglects coherences but makes no assumption of frozen nuclei, and eq 13, which is the contribution from electronic coherences but assumes frozen nuclei during the ionization. Although it is clear that the origin of the oscillatory pattern is the coherence terms, we would like to determine how good the quasistatic approximation is. In particular, if the qsFGR (eq 11) is a good approximation to eq 6, then this simple patch-up can account for the coherent oscillations, and we could avoid the extra propagation that comes with violations of the quasistatic approximation. The qsFGR therefore offers a simple extension of the scFGR that captures the effects of electronic coherences generated internally by the propagation through a region of nonadiabatic dynamics. It is important to note, however, that correctly reproducing these oscillations will require accurate propagation of the magnitude and phase of the coherence $\rho_{ab}(t_d)$.

6. ELECTRONIC COHERENCES CREATED AT CONICAL INTERSECTIONS

We now present simulations of the TRPES signal for a molecular model system representing the branching space of a Conical Intersection (CoIn)[36] by using the exact expression in combination with a fully quantum propagation. We take into account two excited electronic states S_1 and S_2 and the two

DOI: 10.1021/acs.jctc.5b00824
J. Chem. Theory Comput. 2016, 12, 740−752

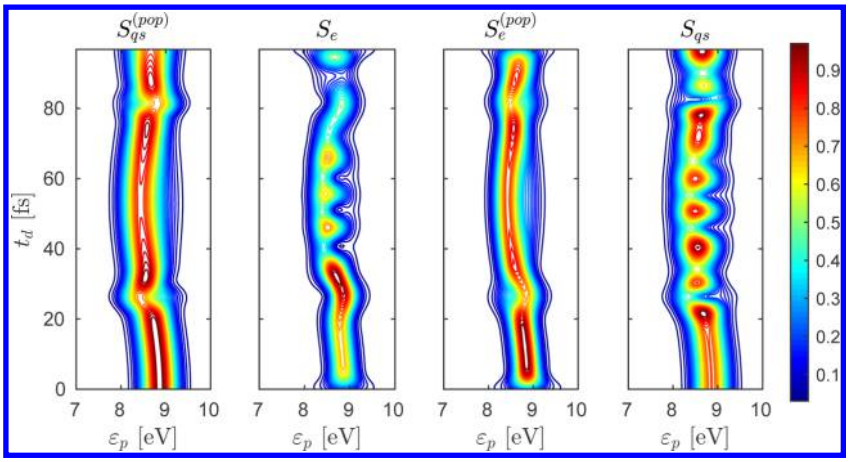

Figure 3. Time-resolved photoelectron spectrum for our model simulated using the qspFGR (eq 12) (far left), the full correlation function and a direct propagation scheme (eq 6) (middle left). Note the prominent oscillations in the latter simulation that reflect the generation of electronic coherence at the CoIn. This beating pattern is clearly absent from the scFGR simulation on the left. To assess the relative importance of (1) the quasistatic approximation and (2) neglecting electronic coherences, we also present the population-only contribution to the correlation-function expression for TRPES (first term in eq 9 (middle left) and compare to the qsFGR (eq 11) (far right). Note the similarity of the exact and quasi-static results. This indicates that the quasistatic approximation is good enough for qualitative purposes provided electronic coherence terms are included.

nuclear coordinates $x = (x_g, x_h)$ that resemble the gradient difference and the derivative coupling vector, respectively. This is the minimal model for a CoIn. The cation states D_0 and D_1 are used as target states to probe the electron dynamics near the CoIn. The cationic potential energy surfaces (PES) are in the same nuclear coordinates but do not possess a CoIn in the space used for the simulations. The ionization energies for D_0 and D_1 at the CoIn point are 6.9 and 7.5 eV, respectively. The molecular Hamiltonian is composed of a Cartesian-type kinetic-energy operator and the corresponding neutral and cation diabatic PESs

$$H = \sum_{j=1}^{4} |j\rangle(\hat{T}_j + \hat{V}_j)\langle j| + |1\rangle\hat{V}_{12}\langle 2| + |2\rangle\hat{V}_{21}\langle 1| \tag{16}$$

where V_1 and V_2 are PESs of the neutral states S_1 and S_2, V_{12} is the diabatic coupling, V_3 and V_4 are the PESs of the cation states D_0 and D_1, and $\hat{T}_j \equiv \sum_{i\in h,g} \frac{-1}{2m}\frac{d^2}{dx_i^2}$ is the nuclear kinetic energy operator acting on electronic state j (we use a reduced mass m of 30000 au or ≈16 amu). The transition dipole moments between the neutral cation states are assumed to be constant with respect to the nuclear coordinate. The time evolution is simulated by wave packet dynamics on a numerical grid using a time stepping scheme (see Appendix B.4). The initial wave function is created by assuming impulsive excitation from the electronic ground state S_0 to the S_2 state.

The time evolution of the populations and the electronic coherence of the neutral states S_1 and S_2 is shown in Figure 4. The wave packet reaches the CoIn within ≈8−15 fs, resulting in an overall population transfer of ≈30%. The electronic coherence build up is maximal at 13.5 fs, when the main fraction of the wave packet has passed the CoIn, followed by a decay of the coherence caused by the different gradients in S_1 and S_2. At 20 fs, the wave packet returns and the coherence rebuilds until the second passage through the CoIn at ≈30 fs. Between 15 and 25 fs the system the systems moves through a region, where coupling V_{12} is negligible and the nuclear wave packets propagate freely on the potential energy surfaces. Note that the term electronic coherence is not clearly defined around

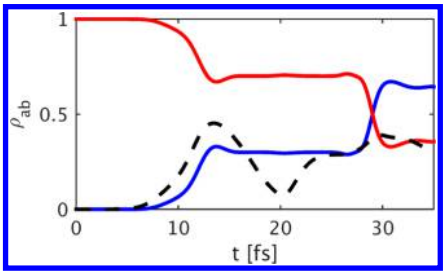

Figure 4. Time evolution of the electronic states populations (S_2 red, S_1 blue) and the coherence magnitude (black, dashed) for the CoIn model.

the CoIn (i.e., around 10 and 30 fs) since the nuclear and electronic wave functions are strongly mixed.

The corresponding TRPES signals calculated for the exact correlation function expression (eq 6) are shown in Figure 5

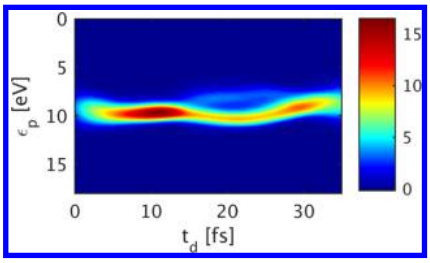

Figure 5. TRPES signal for CoIn with 4 fs FHWM and 20 eV central frequency.

and Figure 6 for two ionization pulse lengths. The signal in Figure 5 is calculated for an ionization pulse, which is long compared to the time scale of the electron dynamics (4 fs fwhm). The splitting of both states is spectrally resolved at around 20 fs (the faint signal at 7 eV stems from the S_1 state). However, the fast oscillations which are expected from the coherence contribution cannot be resolved with the chosen pulse length. The signal in Figure 6 is calculated for an ionization pulse short compared to the time scale of the electron dynamics (0.2 fs fwhm). Here, the spectral features can

DOI: 10.1021/acs.jctc.5b00824
J. Chem. Theory Comput. 2016, 12, 740−752

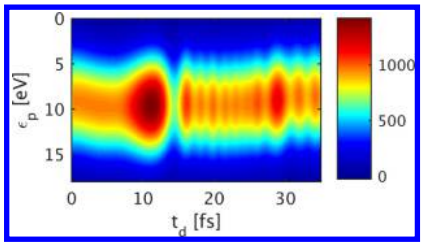

Figure 6. TRPES signal for CoIn using an ionizing pulse with 200 as FWHM and 20 eV central frequency.

not be resolved anymore. The coherent oscillation pattern in the time domain is now fully resolved and visible between 15 and 20 fs. The two ion states are separated by ≈0.6 eV, and they can not be distinguished for the chosen pulse parameters. However, the coherent oscillation pattern is not affected by presence of two ion states. The coherent features of the TRPES signal can be matched in an approximate way against the time evolution of the real part of the coherence $\Re(\rho_{ab})$ (see Appendix B.4 for details) shown in Figure 7(a). The adiabatic

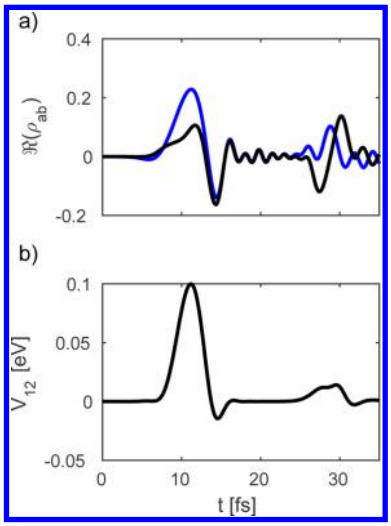

Figure 7. (a) Time evolution of the real part of the electronic coherence in the diabatic basis (blue) and the adiabtic basis (black). (b) Time evolution of the Expectation value of the diabatic coupling (V_{12}).

and diabatic coherence are identical, while the wave packet leaves the coupling region (Figure 7(b)), and the oscillations in the signal stem solely from the electronic states. This can be understood qualitatively by the inspection of eq 9, which separates the contributions to signal into electronic populations and coherences. Assuming the Condon approximation and the limit of short ionization pulses (i.e., the nuclei do not move in the ion states) the second term in eq 9 is proportional to the real part of the coherence $\Re(\rho_{ab})$. Note that a negative $\Re(\rho_{ab})$ depletes the signal contribution from the populations due to destructive interference (as for example at 14.5 fs in Figure 7 and Figure 6).

From the comparison of the signals in Figure 5 and Figure 6, it becomes clear that, in the exact expression, the signal is fully subject to the Fourier uncertainty − time and frequency have to be traded off against each other like in an experiment. However, this is not the case for the qsFGR, where a change in pulse length only affects the spectral but not the temporal resolution.

7. CONCLUSIONS

In this paper we have presented and analyzed a hierarchy of expressions for the calculation of TRPES signals. The main results of the paper are the exact correlation function expression (eq 6) and the qsFGR (eq 11), which extends the widely used scFGR (eq 5) via the inclusion of electronic coherences, accounting for the nuclear overlap between the electronic states. In contrast to the pure population contribution, this term is sensitive to the phase of the ionizing electric field and leads to a beating pattern in the photo electron yield. In model calculations, we have shown that these oscillations can be resolved by the use of attosecond pulses. While the exact correlation function method is mainly intended for use with wave packet propagation protocols on small systems and can be computationally demanding, the qsFGR can be used along with semiclassical molecular dynamics protocols to simulate larger molecular systems. The presented formalism can be applied in an analogous way for the description of photodetachment signals in anions ($A^- \rightarrow A$ rather than $A \rightarrow A^+$).[29]

In previous studies,[24,25] exact wave function propagations were used that are formally identical to our eq 6. Those studies focused on coherent vibrational dynamics and slower electronic population dynamics. Moreover, a common model to consider is one in which each neutral state ionizes to a separate cationic state. In the absence of intersurface coupling in the cationic manifold, the coherence terms for such models vanish identically. Although such coupling had been considered,[25] we can see by eq 9 that the influence of such terms will be limited by the temporal duration of the ionizing pulse. When only electronic population dynamics and coherent vibrational dynamics are important, the qspFGR (which may be approximated by the scFGR) is sufficient to simulate the signal in the quasistatic limit. This approximation is intuitive and frequently employed.[15,16,26] It is only when the two neutral states can both ionize to the same cationic state and the pulses employed are sufficiently short to capture the electronic oscillations that the coherence terms are revealed.

The strategies presented to calculate the signal can readily be interfaced with existing nonadiabatic molecular (quantum) dynamics simulation protocols. The most straightforward way is to evaluate the correlation function eq 6 directly from a time propagation of a wave function in the combined electronic +nuclear space. For example, the molecular system can be propagated in a wave packet approach with the Fourier method[34] in a reduced space of nuclear coordinates[37] including the nonadiabatic couplings.[38,39] The numerical evaluation of the correlation function is then straightforward.[10] Alternatively approximate wave function methods like Multi Configuration Time-Dependent Hartree (MCTDH)[40] can be used to include more vibrational modes and also to evaluate the correlation function. Semiclassical wave packet propagation protocols like Ab Initio Multiple Spawning (AIMS)[31] or Hagendorn wave packets[41] provide access to the nuclear wave function and are thus also suitable for the correlation function method. However, the numerical effort to calculate the signal grows quadratically with the number of time steps, since the correlation function is a function of two variables (t and t'). Moreover, it requires a propagation on the potential energy surface of the ionized molecule. This is in contrast to the various derived FGR expressions, where the numerical effort of the signal calculation only grows linearly with the number of steps. The exact FGR expression (eq 8) requires the eigenstates

DOI: 10.1021/acs.jctc.5b00824
J. Chem. Theory Comput. 2016, 12, 740−752

in the full electronic+nuclear subspace and is thus limited in its applicability. It may however be advantageous in special cases where a diagonalization of an approximate Hamiltonian is feasible (for example in combination with a vibronic coupling Hamiltonian[42]). The linear scaling with respect to the number of time steps might outperform the cost of diagonalization in some cases.

The different types of the FGR presented here neglect the propagation in the ionized states and only require a single time propagation, making them suitable for combination with semiclassical protocols and the description of larger systems. The scFGR, which neglects the contributions of the electronic coherences, has been successfully used in combination with AIMS.[16] An extension to use it with the qsFGR (eq 11) seems straightforward, since AIMS properly includes the necessary nuclear overlap term (eq 13). In principle, the qsFGR expression can also easily be applied to all wave function based methods mentioned above, as long as the nuclear overlap term is accessible. In contrast to the correlation function, the qsFGR does not require time propagation in the ionized molecular states, significantly simplifying its calculation. Simulation protocols like Tully's fewest switch surface hopping (FSSH) method,[32] which treat the nuclei classically, are easy to combine with the scFGR.[28,43] However, the basic version of the FSSH algorithm does not account for the decay of electronic coherences. The result would be an overestimation of coherence contributions to the TRPES signal. Extensions of FSSH, which allow corrections for coherence decay,[44−47] may be used to approximate the nuclear overlap term in eq 13 and combine the class of FSSH methods with the qsFGR. TRPES could provide an experimental test for the various simulation algorithms.

Our model system simulations clearly indicate that a fast buildup of electronic coherences results in an ultrafast oscillation pattern in the time domain of the TRPES signal. Its oscillation period is connected to the energy splitting between the neutral electronic states. A comparison of the different signals yields the conclusion that the qsFGR is a good approximation for the inclusion of electronic coherences beyond the scFGR. However, the quasistatic approximation introduces an unrealistic resolution in the time domain by ignoring the time evolution of the system within the pulse duration. The qsFGR is thus valid for pulses which are short compared to the time scale of the internal dynamics with the scFGR making the additional assumption of neglecting electronic coherences. We have simulated a model system of a CoIn between excited molecular states to demonstrate that the coherent oscillation pattern can be observed in a realistic setting. To obtain an observable coherence, a system with a CoIn in the vincinity of the Franck−Condon point is required to retain a compact wave packet (for example[48−51]). The oscillation pattern is revealed if appropriate subfemtosecond pulses are chosen. The information about the potential energy surface splitting can then be detected through the oscillation period in the time domain instead of the frequency domain. Note that this method accesses information similarly to the resonant linear absorption signal.[22,33]

Finally we note that wave functions at CoIns are known to have a geometric Berry phase[52] that depends on the topology and is independent of the details of the potential surfaces. The Berry phase so far has eluded detection in chemical systems. Spectroscopic signals like TRPES and TRUECARS,[23] which are sensitive to the phase of the pulse and the phase of the electronic coherences, might also provide a new strategy for the experimental observation of geometric phases.

A. PARAMETERS FOR THE ONE-DIMENSIONAL MODEL

The model used in section 5 is defined by the following quantities and parameters (see Table 1).

Table 1. Parameters Used in the Hamiltonian

m	k	d	D	λ	σ_0	σ_T
5100 au	0.01 Ha	0.2 a_0	0.05 Ha	0.01 Ha	0.6 a_0	2.5 fs

Diabatic potential surfaces and couplings are given by

$$\hat{V}_{1/2} = \frac{1}{2}k(x \mp d)^2$$
$$\hat{V}_3 = \frac{1}{2}kx^2 + D$$
$$\hat{V}_{12} = \lambda e^{-x^2} \tag{17}$$

with k, d, and D parameters determining the shape and locations of the harmonic potential surfaces, and λ the coupling strength between the two neutral diabatic states. For our initial state (which is assumed to be the result of some well-timed pumping process), we take a Gaussian nuclear wavepacket on electronic surface 1

$$\phi_0(x) = e^{-\frac{(x+4)^2}{\sigma_0^2}}$$
$$|\Psi_0\rangle = |\phi_0\rangle \otimes |1\rangle \tag{18}$$

B. SIMULATION PROTOCOLS FOR TRPES

In section 5 and Figure 3, we used two different simulation protocols for TRPES with the same model and initial conditions. These protocols, based on eq 6 and eq 12, respectively, both propagate the full nuclear+electronic wave function quantum mechanically. In this Appendix, we will explain in greater detail these two simulation procedures.

B.1. Correlation Function Expression. The photoelectron signal is defined as the energy-resolved, integrated rate of change of the number of photoelectrons which gives the total energy-resolved photoelectron yield

$$S(\varepsilon_{\mathbf{p}}, t_d) = \int dt \frac{d}{dt}\langle \hat{n}_{\mathbf{p}}(t)\rangle \tag{19}$$

It depends on photoelectron energy $\varepsilon_{\mathbf{p}}$ and the delay time t_d of the X-ray pulse relative to state preparation. The signal that we derive generally depends on all parameters describing the ionizing pulse and can be manipulated by pulse shaping, but for simplicity we only explicitly state the t_d dependence. Assuming that the photoelectrons are generated only by interaction with the X-ray pulse (that is, $[\hat{n}_{\mathbf{p}}, \hat{H}_M] = 0$ where $\hat{n}_{\mathbf{p}} = \hat{c}_{\mathbf{p}}^\dagger \hat{c}_{\mathbf{p}}$ is the occupation number of the photoelectron state $|\mathbf{p}\rangle$), we have, from the Heisenberg equation of motion

$$\dot{\hat{n}}_{\mathbf{p}} = -i[\hat{n}_{\mathbf{p}}, H] = -iE_x(t)(\hat{\mu}_{\mathbf{p}} - \hat{\mu}_{\mathbf{p}}^\dagger) \tag{20}$$

where the operator

$$\hat{\mu}_{\mathbf{p}} \equiv \sum_{\alpha a} \hat{\mu}_{\alpha a}^\dagger \hat{c}_{\mathbf{p}} |a\rangle\langle\alpha| \tag{21}$$

DOI: 10.1021/acs.jctc.5b00824
J. Chem. Theory Comput. 2016, 12, 740−752

annihilates a photoelectron and returns the molecule to an un-ionized state.

We will carry out the calculation in Hilbert space since we have an eye toward numerical propagation of the nuclear +electronic wavefunction. We note however that a Liouville space treatment would facilitate the incorporation of environmental degrees of freedom (spectator nuclear modes can also be treated at this level).[28] For simplicity, we will not explicitly incorporate the pumping process but rather take the system to be prepared in a known nonstationary state at time t_0. Since the initial state of the photoelectron is the vacuum $|0\rangle$, the expectation values in eq 20 vanish to first order in E_x. Under the assumption that the ionizing X-ray pulse is well-separated temporally from the preparation process, we may expand the signal to second order in the interaction Hamiltonian to obtain

$$S_e(\varepsilon_p, t_d) = \int dt \int dt' \theta(t - t') E_x(t) E_x(t') \times (\langle \hat{\mu}_p(t) \hat{\mu}_p^\dagger(t') \rangle_0 + \langle \hat{\mu}_p(t') \hat{\mu}_p^\dagger(t) \rangle_0) \quad (22)$$

which may also be read directly from the diagrams in Figure 1. Switching $t \rightarrow t'$ in the second term then yields

$$S_e(\varepsilon_p, t_d) = \int dt \int dt' E_x(t) E_x(t') \langle \hat{\mu}_p(t) \hat{\mu}_p^\dagger(t') \rangle_0 \quad (23)$$

Since the photoelectron and the molecular Hamiltonians commute, we may factor the expectation value and evaluate the photoelectron part yielding eq 6, which may also be written in the frequency domain as

$$S_e(\varepsilon_p, t_d) = \int\int \frac{d\omega d\omega'}{4\pi^2} \tilde{E}_x^*(\omega) \tilde{E}_x(\omega') \times \langle \hat{\mu}(\omega + \omega_x - \varepsilon_p) \hat{\mu}^\dagger(\omega' + \omega_x - \varepsilon_p) \rangle_0 \quad (24)$$

where we have substituted the temporal field envelopes for their Fourier transforms

$$\tilde{E}_x(t) = \int \frac{d\omega}{2\pi} \tilde{E}_x(\omega) e^{-i\omega t} \quad (25)$$

and the conjugate relation for $\tilde{E}_x^*(t)$. The first simulation protocol is based on eq 6 and directly propagates the total nuclear+electronic wavefunction. Thus, we begin with the initial state $|\Psi_0\rangle = |\phi_0\rangle \otimes |1\rangle$ and propagate to some t_{max} in units of δt (we used $\delta t = 6t_h \approx 120$as) via the Lanczos algorithm. This therefore generates a list of wavefunctions

$$|\Psi_{12}(t)\rangle \equiv e^{-i\hat{H}_M t} |\Psi_0\rangle \quad 0 < t < t_{max} \quad (26)$$

where the "12" subscript emphasizes that, since the system begins in state $|1\rangle$ and $\hat{H}_M$ does not couple neutral and ionized electronic states, the propagation is entirely in the manifold of nuclear electronic states. For time t, $0 < t < t_{max}$, we apply the dipole operator, thus generating a list

$$\hat{\mu}^\dagger |\Psi_{12}(t)\rangle \quad 0 < t < t_{max} \quad (27)$$

of the total wavefunction following dipole excitation at time t. In our simulations, we take the dipole operator to be merely map the wavepackets on the neutral surfaces directly to the ionic surface. Thus,

$$\hat{\mu}^\dagger = \sum_{a=1,2} |3\rangle\langle a| \Rightarrow \hat{\mu}^\dagger |\Psi_{12}(t)\rangle = |\phi_{12}(t)\rangle \otimes |3\rangle \quad (28)$$

in our model. The correlation function relevant for the TRPES signal is

$$\langle \hat{\mu}(t) \hat{\mu}^\dagger(t') \rangle = \langle \phi_{12}(t) | e^{-i\hat{E}_3(t-t')} | \phi_{12}(t') \rangle \quad (29)$$

Since the action of the $\hat{\mu}$'s ionizes the system, the remaining exponential propagates the nuclear wavepacket along the ionized surface for time $t - t'$. For every time t', $0 < t' < t_{max} - \delta T$, we therefore generate a matrix of propagated wavepackets

$$|\phi_3(t, t')\rangle = e^{-i\hat{E}_3(t-t')} |\phi_{12}(t')\rangle \quad t' - \delta T < t < t' + \delta T \quad (30)$$

representing propagation in the un-ionized manifold up to time t' and then in the ionized manifold from t' to t (with no restriction on the relative order of t, t'). The restriction $|t-t'| < \delta T$ speeds up the calculation and is valid because the electric field factors $E_x(t(')))$ restrict t to be near t' for temporally limited pulses. In our propagation, we used $\delta T = 30$ fs for a Gaussian field envelope of $\sigma_x = 2.5$ fs. We now obtain the original correlation function by taking the inner product

$$\langle \hat{\mu}(t) \hat{\mu}^\dagger(t') \rangle = \langle \phi_{12}(t) | \phi_3(t, t') \rangle \quad (31)$$

Multiplying this quantity by the field factors defines a two-time function

$$K(t, t') \equiv E_x(t) E_x(t') \langle \phi_{12}(t) | \phi_3(t, t') \rangle \quad (32)$$

and the evaluation of the TRPES signal (eq 6) amounts to a 2D Fourier Transform of this function (actually, a "diagonal" subset of the transformed function $\tilde{K}(\Omega,\Omega')$ in which $\Omega = -\Omega'$). We thus have

$$S(\varepsilon_p, t_d) = K(\varepsilon_p - \omega_x, \omega_x - \varepsilon_p) \quad (33)$$

which depends on time parametrically through the transformed electric field factors. It is this result that is displayed as the S_e in Figure 3. This same basic procedure was also used to generate the S_e^{pop} of Figure 3 except that coherences were projected out.

B.2. Semiclassical and Quasistatic FGR. From eq 9, we make the variable substitutions $\tau = t - t'$, $\bar{t} = \frac{1}{2}(t + t')$ to obtain

$$S_e(\varepsilon_p, t_d) = \int\int \frac{d\omega d\omega'}{2\pi^2} \int d\bar{t} \int d\tau \tilde{E}_x^*(\omega) \tilde{E}_x(\omega') \times e^{-i(\varepsilon_p - \omega_x - \frac{\omega+\omega'}{2})\tau} e^{i(\omega-\omega')\bar{t}} \times \left(\sum_{a\alpha} \langle \hat{M}_{a0}^*\left(\bar{t} + \frac{1}{2}\tau\right) \hat{\mu}_{\alpha a} \hat{M}_{\alpha\alpha}(\tau) \hat{\mu}_{\alpha a}^\dagger \hat{M}_{a0}\left(\bar{t} - \frac{1}{2}\tau\right) \rangle_{\phi_0} + \sum_{a\neq b,\alpha} \langle \hat{M}_{b0}^*\left(\bar{t} + \frac{1}{2}\tau\right) \hat{\mu}_{\alpha b} \hat{M}_{\alpha\alpha}(\tau) \hat{\mu}_{\alpha a}^\dagger \hat{M}_{a0}\left(\bar{t} - \frac{1}{2}\tau\right) \rangle_{\phi_0} \right) \quad (34)$$

In order to simplify the exact transition amplitudes introduced above, we will take the nuclei to be static and neglect the nuclear kinetic energy during the interaction with the ionizing pulse. We term this the quasistatic approximation. For the middle propagators in eq 34, the implications are clear, and we may write

$$\hat{M}_{\alpha\alpha}(\tau) \rightarrow e^{-i\hat{E}_\alpha \tau} \quad (35)$$

DOI: 10.1021/acs.jctc.5b00824
J. Chem. Theory Comput. 2016, 12, 740−752

Table 2. Parameters for the Polynomial Expansions of the Diabatic States of the Two Dimensional Model and Couplings[a]

surf.	c_{00}	c_{10}	c_{01}	c_{20}	c_{11}	c_{02}	c_{30}	c_{21}	c_{12}	c_{03}
V_3	0.260	0.02054	−0.0402	0.3953	−0.03684	0.1665	0.3105	0.1293	−0.2761	0.1213
V_4	0.2862	0.0007407	−0.07507	0.1504	−0.232	0.1897	0.2963	0.2851	−0.3168	0.09636

[a]Given in atomic units.

To handle the remaining transition amplitudes, we propagate under the full Hamiltonian up to the delay time t_d and then under the quasistatic approximation. We thus shift the integration $t^- \rightarrow t^- + t_d$ and write

$$\hat{M}_{a0}\left(t_d + \bar{t} \pm \frac{1}{2}\tau\right) = \hat{M}_{aa}\left(\bar{t} \pm \frac{1}{2}\tau\right)\hat{M}_{a0}(t_d) = \mathrm{e}^{-i\hat{E}_a(\bar{t}\pm\frac{1}{2}\tau)}\hat{M}_{a0}(t_d) \tag{36}$$

where the first equality follows from neglecting the adiabatic coupling after propagation to t_d and the second equality comes directly from neglecting the $\hat{T}$ terms in $\hat{H}_M$. Inserting this into eq 34, we obtain

$$\begin{aligned} S(\varepsilon_{\mathbf{p}}, t_d) = \int\int \frac{d\omega d\omega'}{2\pi^2} \int d\bar{t} \int d\tau \tilde{E}_x^*(\omega)\tilde{E}_x(\omega')\mathrm{e}^{-i(\varepsilon_{\mathbf{p}}-\omega_x-\frac{\omega+\omega'}{2})\tau} \\ \times e^{i(\omega-\omega')(\bar{t}+t_d)} \times \Big(\sum_{a\alpha} \langle \hat{M}_{a0}^*(t_d) e^{i\hat{E}_a(\bar{t}+\frac{1}{2}\tau)}\hat{\mu}_{\alpha a}\mathrm{e}^{-i\hat{E}_\alpha\tau}\hat{\mu}_{\alpha a}^\dagger \\ \times \mathrm{e}^{-i\hat{E}_a(\bar{t}-\frac{1}{2}\tau)}\hat{M}_{a0}(t_d)\rangle_{\phi_0} + \sum_{a\neq b,\alpha} \langle \hat{M}_{b0}^*(t_d) e^{i\hat{E}_b(\bar{t}+\frac{1}{2}\tau)}\hat{\mu}_{\alpha b}\mathrm{e}^{-i\hat{E}_\alpha\tau}\hat{\mu}_{\alpha a}^\dagger \\ \times \mathrm{e}^{-i\hat{E}_a(\bar{t}-\frac{1}{2}\tau)}\hat{M}_{a0}(t_d)\rangle_{\phi_0}\Big) \end{aligned} \tag{37}$$

To carry out the t^- and τ integrations, we now formally act with the transition amplitudes on the initial nuclear wavepacket. This propagates the nuclear wavepacket to time t_d. We then take the nuclear wavepacket as frozen for the integrations, allowing us to replace the $\mathcal{E}$'s with their expectation values over the frozen wavepacket

$$\hat{M}_{a0}(t_d)|\phi_0\rangle = c_a(t_d)|\phi_a(t_d)\rangle \tag{38}$$

with $c_a(t)$ the time-dependent propability amplitude associated with electronic state $|a\rangle$ and $\phi_a(t_d)$ the nuclear wavepacket on electronic surface a at time t_d and replace the adiabatic potentials with

$$\begin{aligned} \mathcal{E}_a(t_d) &\equiv \langle\phi_a(t_d)|\hat{E}_a|\phi_a(t_d)\rangle \\ \mathcal{E}_\alpha(t_d) &\equiv \langle\phi_{\alpha a}(t_d)|\hat{E}_\alpha|\phi_{\alpha a}(t_d)\rangle \end{aligned} \tag{39}$$

The second equation follows upon defining the nuclear wavepacket after dipolar excitation

$$\hat{\mu}_{\alpha a}^\dagger|\phi_a(t_d)\rangle \equiv \mu_{\alpha a}^*(t_d)|\phi_{\alpha a}(t_d)\rangle \tag{40}$$

Such an expression is possible to write because the dipole operator $\hat{\mu}_{\alpha a}^\dagger$ simply maps the original nuclear wavefunction $|\phi_a(t_d)\rangle$ to a new wavefunction $|\phi_{\alpha a}(t_d)\rangle$, the details of which reflect the dependence of the dipole on the nuclear coordinates. The time-dependence of the resulting c-number $\mu_{\alpha a}^*$ is necessary since the dipole is not unitary and the transformed nuclear wavefunction has a time-dependent normalization which is absorbed into the $\mu_{\alpha a}^*$. Thus, in this approximation, the vibronic states can be altered by the dipole operator but not by the time propagators. Note that if, as in the Condon approximation, the nuclear wavefunction is unaffected by the electronic dipole operator, we have $|\phi_{\alpha a}(t_d)\rangle = |\phi_a(t_d)\rangle$ and $\mu_{\alpha a}^*(t_d) = \mu_{\alpha a}^*$ and things simplify somewhat. Inserting eqs 38−40 into 37, we may now carry out the time integrations since all operators have been replaced by their expectation values yielding eq 11.

The second simulation protocol used is based on eq 12. We first note that our uniform dipole operator in the Condon approximation allows us to drop the $\mu_{\alpha a}$ factor. Using the same list

$$|\Psi_{12}(t)\rangle \equiv \mathrm{e}^{-i\hat{H}_M t}|\Psi_0\rangle \quad 0 < t < t_{\max} \tag{41}$$

generated in the first protocol, we project onto a neutral state $|a\rangle$, defining

$$\langle a|\Psi_{12}(t)\rangle = c_a(t)|\phi_a(t)\rangle \tag{42}$$

in accordance with eq 38. We now take expectation values of the electronic energies over this nuclear wavepacket

$$\begin{aligned} \langle\phi_a(t)|\hat{\mathcal{E}}_a|\phi_a(t)\rangle &\equiv \mathcal{E}_a(t) \\ \langle\phi_a(t)|\hat{\mathcal{E}}_\alpha|\phi_a(t)\rangle &\equiv \mathcal{E}_\alpha(t) \end{aligned} \tag{43}$$

Combined with the populations $|c_a(t)|^2$, these expectation values are then all the ingredients to eqs 12, 13, and therefore 11. For the ionizing field amplitude profile $E_x(\omega)$, we use a Gaussian spectral field envelope of width $\sigma_\omega^{-1} \approx 2.5$ fs for comparison to the temporal field envelope used in the previous section. We thereby generate the qspFGR of Figure 3. Note that both simulation protocols begin with the same wave function propagated in the neutral manifold. This propagation is what generates the coherences that lead to the oscillations in the photoelectron signal. The correlation-function protocol also requires propagation in the ionized manifold as well as including electronic coherences which are omitted in the qsFGR (the quasistatic assumption).

B.3. Parameters for CoIn model (Figures 4−7). We use a two-dimensional model system inspired by the S_2−S_1 CoIn in acrolein.[10,28,53] The system has been chosen as a role model to obtain realistic parameters for the energy splittings between the PESs and the couplings. The adiabatic and diabatic states were calculated in the vinicinty of the CoIn with the program package MOLPRO[54] at the CASSCF(6/5)/6-31+G*level of theory. The two coordinates of the system, x_h and x_g, correspond to the orthonormal versions of the derivative coupling vector and the gradient difference vector, respectively. The diabatic potential energy surfaces and the diabatic couplings have been calculated on a 9 × 9 grid with maximum displacements of ±0.4. The CoIn is in the origin of the coordinate system. The resulting data is fitted to a third order polynomial:

$$\begin{aligned} f_1(x_h, x_g) = c_{00} + c_{10}x_h + c_{01}x_g + c_{20}x_h^2 + c_{11}x_hx_g + c_{02}x_g^2 \\ + c_{30}x_h^3 + c_{21}x_h^2x_g + c_{12}x_hx_g^2 + c_{03}x_g^3 \end{aligned} \tag{44}$$

The cation states D_0 and D_1 are in the same nuclear coordinate system and determined at the CASSCF(5/5)/6-31+G*level of theory. The PES for the D_0 state is fitted with eq 44. The ion state D_1 (V_4) is fitted by a fourth order polynomial:

$$f_2(x_h, x_g) = f_1(x_h, x_g) + c_{40}x_h^4 + c_{31}x_h^3x_g + c_{22}x_h^2x_g^2 + c_{13}x_hx_g^3 + c_{04}x_g^4 \tag{45}$$

DOI: 10.1021/acs.jctc.5b00824
J. Chem. Theory Comput. 2016, 12, 740−752

The respective parameter sets c_{ij} for the ion states Vs are given in Table 2. The additional fourth order parameters for V_4 are given in Table 3. The parameters for the two neutral states as

Table 3. Parameters for the Fourth Order Parameters of V_4 (Eq 45)[a]

c_{40}	c_{31}	c_{22}	c_{13}	c_{04}
0.4607	0.4479	0.2463	−0.1592	0.01413

[a]Given in atomic units.

well as a graphical representation are given in ref 23. The polynomial allows for extrapolation of the data to a wider parameter range, necessary to run the wave packet simulations. The potential energy surfaces of the cation states are shown in

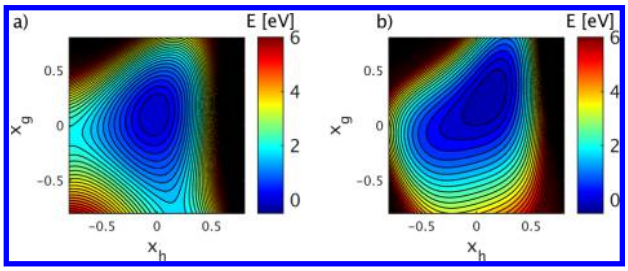

Figure 8. Potential energy surfaces of the cation states a) V_3 and b) V_4.

Figure 8. The diabatic coupling V_{12} is created by eq 44 and shaped by Gaussian functions

$$V_{12} = f_1(x_h, x_g)h(x_h)\exp\left(\frac{-x_g^2}{0.08}\right) \tag{46}$$

where $h(x_h)$ is

$$h(x_h) = \begin{cases} \exp\left(-\frac{x_h^2}{0.18}\right) & x_h < 0 \\ \exp\left(-\frac{x_h^2}{0.045}\right) & x_h \geq 0 \end{cases} \tag{47}$$

The Gaussian envelope lets the diabatic coupling term vanish in areas far from the CoIn and diabatic states become identical to the adiabatic states. The coefficients can be found in ref 23.

B.4. Wave Packet Propagation. The wave packet propagation is calculated by time stepping

$$\psi(x, t + \Delta t) = \exp(-iH\Delta t)\psi(x, t) \tag{48}$$

with the Short Iterative Lanczos (SIL) method[34] and a step size of Δt = 2 au (≈50 as). The corresponding diabatic wave function is expressed in terms of the electronic states

$$\psi(x, t) = (\phi_1(x, t) \;\; \phi_2(x, t) \;\; \phi_3(x, t) \;\; \phi_4(x, t))^T \tag{49}$$

with the normalization $\langle\psi|\,\psi\rangle = 1$. The resulting time series $\psi(x,t)$ is used subsequently in the signal calculation. The dipole operator used to create ion states is assumed to be within in the Condon approximations and reads

$$\hat{\mu}^\dagger = (|3\rangle + |4\rangle)(\langle 1| + \langle 2|) \tag{50}$$

The reduced electronic density matrix of the neutral states is obtained by integrating over the nuclear degrees of freedom

$$\rho_{el} = \mathrm{Tr}_n(\rho) = \begin{pmatrix} \langle\phi_1|\phi_1\rangle & \langle\phi_1|\phi_2\rangle \\ \langle\phi_2|\phi_1\rangle & \langle\phi_2|\phi_2\rangle \end{pmatrix} \tag{51}$$

where $\rho_{ii} = \langle\phi_i|\phi_i\rangle$ is the population of the ith electronic state, and $\rho_{12} = \langle\phi_1|\phi_2\rangle$ the coherence between the two states.

The adiabatic wave function is obtained by the unitary transformation $U(x)$ that diagonalizes the diabatic PESs

$$\begin{pmatrix} \Psi_1(x, t) \\ \Psi_2(x, t) \end{pmatrix} = \begin{pmatrix} \cos(\theta(x)) & \sin(\theta(x)) \\ -\sin(\theta(x)) & \cos(\theta(x)) \end{pmatrix}\begin{pmatrix} \phi_1(x, t) \\ \phi_2(x, t) \end{pmatrix} \tag{52}$$

with the mixing angle θ

$$\tan 2\theta(x) = \frac{1}{2}\frac{V_{12}(x)}{V_1(x) - V_2(x)} \tag{53}$$

AUTHOR INFORMATION

Corresponding Authors

*E-mail: kcbennet@uci.edu (K.B.).
*E-mail: mkowalew@uci.edu (M.K.).
*E-mail: smukamel@uci.edu (S.M.).

Notes

The authors declare no competing financial interest.

ACKNOWLEDGMENTS

S.M. gratefully acknowledges the support of Freiburg Institute for Advanced Studies (FRIAS), University of Freiburg, Germany. The support of the Chemical Sciences, Geosciences, and Biosciences division, Office of Basic Energy Sciences, Office of Science, U.S. Department of Energy through award No. DE-FG02-04ER15571 as well as from the National Science Foundation (grant CHE-1361516) is gratefully acknowledged. The computational resources and the support for Kochise Bennett was provided by DOE. M.K. gratefully acknowledges support from the Alexander von Humboldt foundation through the Feodor Lynen program.

REFERENCES

(1) Carlson, T. A. Photoelectron Spectroscopy. *Annu. Rev. Phys. Chem.* **1975**, *26*, 211−234.
(2) Stolow, A.; Bragg, A. E.; Neumark, D. M. Femtosecond Time-Resolved Photoelectron Spectroscopy. *Chem. Rev.* **2004**, *104*, 1719−1758.
(3) Polli, D.; Altoe, P.; Weingart, O.; Spillane, K. M.; Manzoni, C.; Brida, D.; Tomasello, G.; Orlandi, G.; Kukura, P.; Mathies, R. A.; Garavelli, M.; Cerullo, G. Conical intersection dynamics of the primary photoisomerization event in vision. *Nature* **2010**, *467*, 440−443.
(4) Rinaldi, S.; Melaccio, F.; Gozem, S.; Fanelli, F.; Olivucci, M. Comparison of the isomerization mechanisms of human melanopsin and invertebrate and vertebrate rhodopsins. *Proc. Natl. Acad. Sci. U. S. A.* **2014**, *111*, 1714−1719.
(5) Barbatti, M.; Granucci, G.; Persico, M.; Ruckenbauer, M.; Vazdar, M.; Eckert-Maksić, M.; Lischka, H. The on-the-fly surface-hopping program system Newton-X: Application to ab initio simulation of the nonadiabatic photodynamics of benchmark systems. *J. Photochem. Photobiol., A* **2007**, *190*, 228−240.
(6) Barbatti, M.; Aquino, A. J. A.; Szymczak, J. J.; Nachtigallová, D.; Hobza, P.; Lischka, H. Relaxation mechanisms of UV-photoexcited DNA and RNA nucleobases. *Proc. Natl. Acad. Sci. U. S. A.* **2010**, *107*, 21453−21458.

DOI: 10.1021/acs.jctc.5b00824
J. Chem. Theory Comput. 2016, 12, 740−752

(7) Sobolewski, A. L.; Domcke, W.; Dedonder-Lardeux, C.; Jouvet, C. Excited-state hydrogen detachment and hydrogen transfer driven by repulsive 1$\pi\sigma$*states: A new paradigm for nonradiative decay in aromatic biomolecules. *Phys. Chem. Chem. Phys.* **2002**, *4*, 1093−1100.
(8) Meyer, H. The molecular hamiltonian. *Annu. Rev. Phys. Chem.* **2002**, *53*, 141−172.
(9) Worth, G. A.; Cederbaum, L. S. Beyond Born-Oppenheimer: molecular dynamics through a conical intersection. *Annu. Rev. Phys. Chem.* **2004**, *55*, 127−158.
(10) Kowalewski, M.; Mukamel, S. Stimulated Raman signals at conical intersections: Ab initio surface hopping simulation protocol with direct propagation of the nuclear wave function. *J. Chem. Phys.* **2015**, *143*, 044117.
(11) Raab, A.; Worth, G. A.; Meyer, H. D.; Cederbaum, L. S. Molecular dynamics of pyrazine after excitation to the S2 electronic state using a realistic 24-mode model Hamiltonian. *J. Chem. Phys.* **1999**, *110*, 936.
(12) Oliver, T. A. A.; Lewis, N. H. C.; Fleming, G. R. Correlating the motion of electrons and nuclei with two-dimensional electronic-vibrational spectroscopy. *Proc. Natl. Acad. Sci. U. S. A.* **2014**, *111*, 10061−10066.
(13) Timmers, H.; Li, Z.; Shivaram, N.; Santra, R.; Vendrell, O.; Sandhu, A. Coherent Electron Hole Dynamics Near a Conical Intersection. *Phys. Rev. Lett.* **2014**, *113*, 113003.
(14) McFarland, B. K.; Farrell, J. P.; Miyabe, S.; Tarantelli, F.; Aguilar, A.; Berrah, N.; Bostedt, C.; Bozek, J. D.; Bucksbaum, P. H.; Castagna, J. C.; Coffee, R. N.; Cryan, J. P.; Fang, L.; Feifel, R.; Gaffney, K. J.; Glownia, J. M.; Martinez, T. J.; Mucke, M.; Murphy, B.; Natan, A.; Osipov, T.; Petrović, V. S.; Schorb, S.; Schultz, T.; Spector, L. S.; Swiggers, M.; Tenney, I.; Wang, S.; White, J. L.; White, W.; Gühr, M. Ultrafast X-ray Auger probing of photoexcited molecular dynamics. *Nat. Commun.* **2014**, *5*, 4235.
(15) Ho, J.-W.; Yen, H.-C.; Chou, W.-K.; Weng, C.-N.; Cheng, L.-H.; Shi, H.-Q.; Lai, S.-H.; Cheng, P.-Y. Disentangling Intrinsic Ultrafast Excited-State Dynamics of Cytosine Tautomers. *J. Phys. Chem. A* **2011**, *115*, 8406−8418.
(16) Thompson, A. L.; Martinez, T. J. Time-resolved photoelectron spectroscopy from first principles: Excited state dynamics of benzene. *Faraday Discuss.* **2011**, *150*, 293−311.
(17) Hentschel, M.; Kienberger, R.; Spielmann, C.; Reider, G. A.; Milosevic, N.; Brabec, T.; Corkum, P.; Heinzmann, U.; Drescher, M.; Krausz, F. Attosecond metrology. *Nature* **2001**, *414*, 509−513.
(18) von den Hoff, P.; Siemering, R.; Kowalewski, M.; de Vivie-Riedle, R. Electron Dynamics and Its Control in Molecules: From Diatomics to Larger Molecular Systems. *IEEE J. Sel. Top. Quantum Electron.* **2011**, *18*, 119−129.
(19) Ding, Y.; Huang, Z.; Ratner, D.; Bucksbaum, P.; Merdji, H. Generation of attosecond x-ray pulses with a multicycle two-color enhanced self-amplified spontaneous emission scheme. *Phys. Rev. Spec. Top.−Accel. Beams* **2009**, *12*, 060703.
(20) Helml, W.; Maier, A. R.; Schweinberger, W.; Grguraš, I.; Radcliffe, P.; Doumy, G.; Roedig, C.; Gagnon, J.; Messerschmidt, M.; Schorb, S.; Bostedt, C.; Grüner, F.; DiMauro, L. F.; Cubaynes, D.; Bozek, J. D.; Th, T.; Costello, J. T.; Meyer, M.; Coffee, R.; Düsterer, S.; Cavalieri, A. L.; Kienberger, R. Measuring the temporal structure of few-femtosecond free-electron laser X-ray pulses directly in the time domain. *Nat. Photonics* **2014**, *8*, 950−957.
(21) Popmintchev, T.; Chen, M.-C.; Arpin, P.; Murnane, M. M.; Kapteyn, H. C. The attosecond nonlinear optics of bright coherent X-ray generation. *Nat. Photonics* **2010**, *4*, 822−832.
(22) Dorfman, K. E.; Bennett, K.; Mukamel, S. Detecting electronic coherence by multidimensional broadband stimulated x-ray Raman signals. *Phys. Rev. A: At., Mol., Opt. Phys.* **2015**, *92*, 023826.
(23) Kowalewski, M.; Bennett, K.; Dorfman, K. E.; Mukamel, S. Catching Conical Intersections in the Act: Monitoring Transient Electronic Coherences by Attosecond Stimulated X-Ray Raman Signals. *Phys. Rev. Lett.* **2015**, *115*, 193003.
(24) Seel, M.; Domcke, W. Model studies on femtosecond time-resolved ionization spectroscopy of excited-state vibrational dynamics and vibronic coupling. *Chem. Phys.* **1991**, *151*, 59−72.
(25) Hahn, S.; Stock, G. Efficient calculation of femtosecond time-resolved photoelectron spectra: method and application to the ionization of pyrazine. *Phys. Chem. Chem. Phys.* **2001**, *3*, 2331−2336.
(26) Kuhlman, T. S.; Glover, W. J.; Mori, T.; Møller, K. B.; Martínez, T. J. Between ethylene and polyenes-the non-adiabatic dynamics of cis-dienes. *Faraday Discuss.* **2012**, *157*, 193−212.
(27) Trabs, P.; Buchner, F.; Ghotbi, M.; Lübcke, A.; Ritze, H.-H.; Vrakking, M. J. J.; Rouzée, A. Time-, angle- and kinetic-energy-resolved photoelectron spectroscopy of highly excited states of NO. *J. Phys. B: At., Mol. Opt. Phys.* **2014**, *47*, 124016.
(28) Bennett, K.; Kowalewski, M.; Mukamel, S. Probing electronic and vibrational dynamics in molecules by time-resolved photoelectron, Auger-electron, and X-ray photon scattering spectroscopy. *Faraday Discuss.* **2015**, *177*, 405−428.
(29) Chen, X.; Bradforth, S. E. The ultrafast dynamics of photodetachment. *Annu. Rev. Phys. Chem.* **2008**, *59*, 203−231.
(30) Zhang, J.; Nakajima, T. Influence of Coulomb potential for photoionization of H atoms in an elliptically polarized laser field: Velocity gauge versus length gauge. *Phys. Rev. A: At., Mol., Opt. Phys.* **2008**, *77*, 043417.
(31) Ben-Nun, M.; Quenneville, J.; Martínez, T. J. Ab Initio Multiple Spawning: Photochemistry from First Principles Quantum Molecular Dynamics. *J. Phys. Chem. A* **2000**, *104*, 5161−5175.
(32) Hammes-Schiffer, S.; Tully, J. C. Proton transfer in solution: Molecular dynamics with quantum transitions. *J. Chem. Phys.* **1994**, *101*, 4657−4667.
(33) Rahav, S.; Mukamel, S. Multidimensional attosecond photoelectron spectroscopy with shaped pulses and quantum optical fields. *Phys. Rev. A: At., Mol., Opt. Phys.* **2010**, *81*, 063810.
(34) Tannor, D. J. *Introduction to Quantum Mechanics: A Time-Dependent Perspective*; University Science Books: 2006; pp 145−178.
(35) Oana, C. M.; Krylov, A. I. Dyson orbitals for ionization from the ground and electronically excited states within equation-of-motion coupled-cluster formalism: Theory, implementation, and examples. *J. Chem. Phys.* **2007**, *127*, 234106.
(36) Domcke, W.; Yarkony, D. R.; Köppel, H. *Conical Intersections*; World Scientific: 2011; Vol. *17*.
(37) Kowalewski, M.; Mikosch, J.; Wester, R.; de Vivie-Riedle, R. Nucleophilic Substitution Dynamics: Comparing Wave Packet Calculations with Experiment. *J. Phys. Chem. A* **2014**, *118*, 4661−4669.
(38) Fingerhut, B. P.; Geppert, D.; de Vivie-Riedle, R. Ultrafast dissociation pathways of diphenylmethyl chloride to generate reactive carbo cations. *Chem. Phys.* **2008**, *343*, 329−339.
(39) von den Hoff, P.; Thallmair, S.; Kowalewski, M.; Siemering, R.; de Vivie-Riedle, R. Optimal control theory - closing the gap between theory and experiment. *Phys. Chem. Chem. Phys.* **2012**, *14*, 14460.
(40) Meyer, H.-D. Studying molecular quantum dynamics with the multiconfiguration time-dependent Hartree method. *WIREs Comput. Mol. Sci.* **2012**, *2*, 351−374.
(41) Bourquin, R.; Gradinaru, V.; Hagedorn, G. A. Non-adiabatic transitions near avoided crossings: theory and numerics. *J. Math. Chem.* **2012**, *50*, 602−619.
(42) Köppel, H.; Domcke, W.; Cederbaum, L. S. *Multimode Molecular Dynamics Beyond the Born-Oppenheimer Approximation* **1984**, *57*, 59−246.
(43) Humeniuk, A.; Wohlgemuth, M.; Suzuki, T.; Mitrić, R. Time-resolved photoelectron imaging spectra from non-adiabatic molecular dynamics simulations. *J. Chem. Phys.* **2013**, *139*, 134104.
(44) Landry, B. R.; Subotnik, J. E. How to recover Marcus theory with fewest switches surface hopping: Add just a touch of decoherence. *J. Chem. Phys.* **2012**, *137*, 22A513.
(45) Granucci, G.; Persico, M.; Zoccante, A. Including quantum decoherence in surface hopping. *J. Chem. Phys.* **2010**, *133*, 134111.
(46) Käb, G. Fewest Switches Adiabatic Surface Hopping As Applied to Vibrational Energy Relaxation†. *J. Phys. Chem. A* **2006**, *110*, 3197−3215.

DOI: 10.1021/acs.jctc.5b00824
J. Chem. Theory Comput. 2016, 12, 740−752

(47) Martens, C. C. Communication: Fully coherent quantum state hopping. *J. Chem. Phys.* **2015**, *143*, 141101.
(48) Tao, H.; Allison, T. K.; Wright, T. W.; Stooke, A. M.; Khurmi, C.; van Tilborg, J.; Liu, Y.; Falcone, R. W.; Belkacem, A.; Martinez, T. J. Ultrafast internal conversion in ethylene. I. The excited state lifetime. *J. Chem. Phys.* **2011**, *134*, 244306.
(49) Kochman, M. A.; Tajti, A.; Morrison, C. A.; Miller, R. J. D. Early Events in the Nonadiabatic Relaxation Dynamics of 4-(N,N-Dimethylamino)benzonitrile. *J. Chem. Theory Comput.* **2015**, *11*, 1118−1128.
(50) Tamura, H.; Nanbu, S.; Ishida, T.; Nakamura, H. Ab initio nonadiabatic quantum dynamics of cyclohexadiene/hexatriene ultrafast photoisomerization. *J. Chem. Phys.* **2006**, *124*, 084313.
(51) Horio, T.; Fuji, T.; Suzuki, Y.-I.; Suzuki, T. Probing Ultrafast Internal Conversion through Conical Intersection via Time-Energy Map of Photoelectron Angular Anisotropy. *J. Am. Chem. Soc.* **2009**, *131*, 10392−10393.
(52) Xiao, D.; Chang, M.-C.; Niu, Q. Berry phase effects on electronic properties. *Rev. Mod. Phys.* **2010**, *82*, 1959−2007.
(53) Lee, A. M. D.; Coe, J. D.; Ullrich, S.; Ho, M. L.; Lee, S. J.; Cheng, B. M.; Zgierski, M. Z.; Chen, I. C.; Martinez, T. J.; Stolow, A. Substituent Effects on Dynamics at Conical Intersections: α,β-Enones. *J. Phys. Chem. A* **2007**, *111*, 11948−11960.
(54) Werner, H.-J. et al. MOLPRO, version 2010.1, a package of ab initio programs; 2010. See http://www.molpro.net (accessed 11/01/2015).

DOI: 10.1021/acs.jctc.5b00824
J. Chem. Theory Comput. 2016, 12, 740−752